NUMERICAL ANALYSIS OF TURBULENT RAYLEIGH-BÉNARD CONVECTION ON THE BASE OF THE LARGE EDDY SIMULATION TECHNIQUE

A.G. Abramov, N.G. Ivanov and E.M. Smirnov

Saint-Petersburg State Polytechnic University, Saint-Petersburg, Russia

e-mail: aerofmf@citadel.stu.neva.ru

Introduction

Nowadays there are wide possibilities to perform numerical studies of turbulent natural convection flows on the base of 3D unsteady formulations [1]. *Direct Numerical Simulation* (DNS) is the most attractive and reliable approach for getting a detailed knowledge on convection [2, 3]. However, DNS applications are practically limited by the case of simplified geometry and/or the Rayleigh numbers not exceeding 10^8. Results of unsteady computations based on the *Reynolds-Averaged Navier-Stokes* (RANS) equations are very sensitive to the turbulence model choice. Expectations for covering the range of high Rayleigh numbers are traditionally concerned with *Large Eddy Simulation* (LES). However, in case of LES applications to wall-bounded flows the major difficulties are associated with the treatment of the near-wall layers [4, 5]. Typically approximate wall boundary conditions (wall functions) are used to keep reasonable computational grids. But wall functions introduce further empiricism in calculations and may lead to uncertain results. In order to overcome these drawbacks recent works proposed hybrid techniques combining RANS and LES approaches [5].

The present work is aimed at numerical simulation of strongly turbulent Rayleigh-Bénard (RB) convection in confined enclosures of aspect ratio 1. Mercury and water, characterized by essentially different Prandtl numbers, have been chosen as test fluids. Turbulence modelling is performed with a RANS/LES hybridization involving the equation of the kinetic energy of unresolved motion. Results of computations are presented in comparison with experimental data.

Problem formulation

The problem under consideration is thermal convection in confined cubic and cylindrical cells of aspect ratio 1 heated from below. The cell height H is taken as a length scale. The cold top and hot bottom plates are maintained at constant temperature (T_c and T_h respectively), the gravity vector, $\mathbf{g}$, points downwards. The temperature difference $\Delta T = T_h - T_c$ is used to introduce a normalized temperature. The lateral walls of the cells are adiabatic. No-slip velocity boundary conditions are imposed on all the walls. The buoyancy velocity, $V_b = (g\beta\Delta TH)^{1/2}$, is taken as a velocity scale, and the ratio H/V_b serves as a time scale. With given geometry, the flow dynamics in the cells is fully determined by values of the Prandtl number, $Pr = \nu/a$, and the Rayleigh number, $Ra = g\beta\Delta TH^3/(\nu a)$. Below turbulent regimes of RB mercury convection ($Pr = 0.025$) are considered for the cylindrical cell, and turbulent water convection at $Pr = 7$ is studied for the cubic cell.

Mathematical model and computational aspects

Resolved scales of turbulent flow under consideration are described by the averaged/filtered Navier-Stokes equations with the Boussinesq approximation for incorporation of buoyancy effects. The unresolved scales activity is taken into account using a recently developed hybrid RANS/LES technique based on the one-equation model for the kinetic energy of unresolved motion [1, 6]. In this technique, RANS/LES region switching is controlled via a

comparison of dissipation rates given by a RANS model and a subgrid-scale model of LES. Note that this technique ought to be classified as a non-standard *Detached Eddy Simulation* (DES) [7], since the RANS zone, unlike to the standard DES [5], covers only the near-wall part of a high-shear boundary layer. In other words, it can be treated as an alternative to the use of wall functions [8].

Computations have been carried out using a well-validated in-house code (named SINF), which is under long-time development at the Department of Hydro- and Aerodynamics of the St.-Petersburg State Polytechnic University. This advanced 3D Navier-Stokes solver is based on the second-order finite-volume spatial discretization using the cell-centred variable arrangement and body-fitted block-structured grids. The discretization of time derivatives is done with a three-time-level, second-order implicit scheme. The artificial-compressibility method is applied at each time step. The code is in wide use for solving both fundamental and industrial problems. Additional details of the solver can be found elsewhere [9].

In the present computations, the cylindrical cell was covered by a two-block grid and the cubic cell was covered by a single-block grid. Both the grids, consisting of about 160,000 cells, were clustered to the walls so that the normalized time-averaged near-wall coordinate for the first computational point, y^+, was less than unity. As a result of preliminary study, the non-dimensional time step was set to 0.1. For both the configurations, the computations for the first run were started from zero velocity and T = 0.5 temperature fields. After a transient period of 100 time units, a statistically developed regime was obtained. For the other runs, the computations were started from an instantaneous field saved for the first case and transient periods of about 50 time units were passed. Samples computed after the transient periods were 200 to 300 time units.

Results and discussion

The mercury convection was studied for the Rayleigh number ranging from 10^8 to 5×10^9, and the water convection was simulated at $Ra = 5\times10^8$ and 5×10^9. The computations reproduced clearly prominent features of turbulent RB convection in confined enclosures. First feature, typical for low aspect ratio tanks, consists in formation of a stable large-scale circulation that spans the whole height of the cell.

The presence of the global circulation in the cubic enclosure is illustrated in Fig. 1a ($Ra = 5\times10^9$). It can be seen that two isosurfaces of vertical velocity corresponding to the absolute value of 0.05 are mostly located on different sides with respect to a cubic diagonal plane. This result is in accordance with experimental observations [10, 11]. On the other hand, in

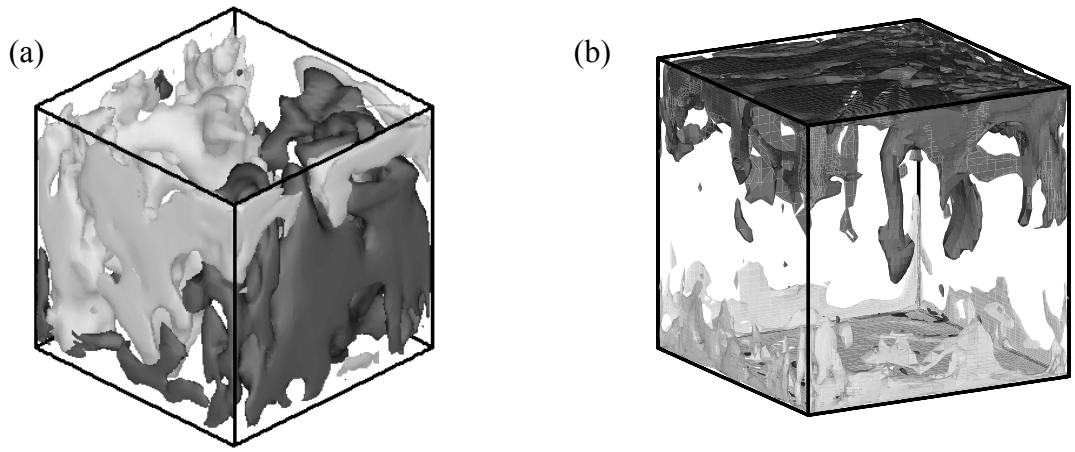

Fig. 1. Water convection at $Ra = 5\times10^9$: (a) isosurfaces of vertical velocity w = 0.05 (black) and w = -0.05 (gray), and (b) temperature isosurfaces T = 0.45 (black) and T = 0.55 (gray)

case of the cylindrical cell the global structure changed slowly its orientation in time that could be quite expected due to the axial symmetry of the cell. The intensive large-scale motion induced a stable flow that can be treated as a "wind" sweeping along the horizontal walls of the cell. Thus the global circulation strongly affects viscous boundary layers forming near the isothermal walls.

Quantitatively, the global circulation can be characterized by the maximum horizontal temperature difference, ΔT_h, and by the maximum vertical velocity difference, Δw_h, both evaluated at the mid-plane. The present computations showed that for mercury ΔT_h and Δw_h are about three times larger than for water, as listed in Table 1. For both the fluids, ΔT_h and Δw_h decrease with increasing the Rayleigh number if $Ra \geq 10^8$. Note that DNS data reported in [12] indicated that ΔT_h and Δw_h are almost independent of Ra for the range $Ra \leq 10^6$. This result was reproduced in our test computations of mercury convection [8, 13] as well (see Table 1). Following [12], we introduced a scale velocity of the global circulation, V_g, determined as a half of Δw_h, the latter is extracted from the computed data. Results of evaluation of the Reynolds number, $Re_g = V_g \cdot H / \nu$, given in Table 1, agree well with scaling laws obtained in experiments [14, 15].

Table 1

Characteristics of turbulent R-B convection

Approach	Ra	Pr	ΔT_h	Δw_h	Re_g	δ_T	δ_V
DNS	10^5	0.025	0.560	1.57	1560	0.170	0.0240
DNS	10^6	0.025	0.556	1.53	4807	0.090	0.0120
RANS/LES	10^8	0.025	0.458	1.09	34785	0.024	0.0035
same	5×10^8	0.025	0.430	1.05	74953	0.018	0.0023
same	8.7×10^8	0.025	0.405	0.99	93274	0.014	0.0020
same	5×10^9	0.025	0.358	0.96	214663	0.009	0.0014
same	5×10^8	7	0.177	0.42	1787	0.014	0.0170
same	5×10^9	7	0.133	0.38	5078	0.008	0.0120

Another remarkable feature of the turbulent RB convection is associated with vertical movement of fluid portions (thermal plumes). As shown in Fig. 1b, these coherent mushroom-head structures arise from the top and bottom temperature boundary layers and move in the opposite wall direction. Strong turbulent mixing in the flow core prevents thermals to move through the central part of the cell. As a result, most of thermals are localized near the lateral walls including regions of rising and descending large-scale motion. In mercury, due to a larger thermal diffusivity, activity of plumes is noticeably weaker, and they were registered in our computations only for $Ra \geq 10^8$ [6, 8].

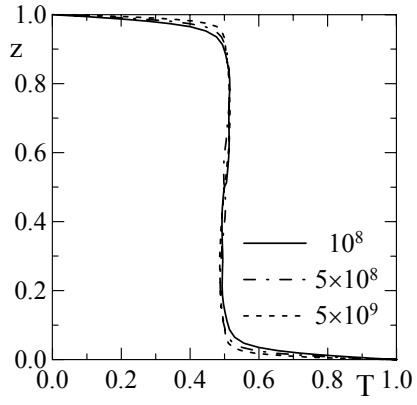

Fig. 2. Effect of the Rayleigh number on temperature profiles in mercury

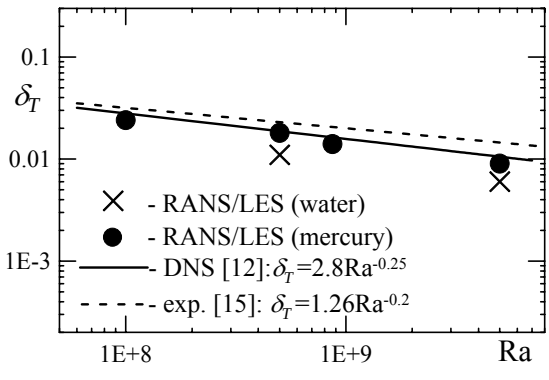

Fig. 3. Thermal boundary layer thickness versus Rayleigh number. Comparison with extrapolations of known experimental and DNS data for mercury to higher Ra

Figure 2 shows temperature profiles in mercury obtained for three Ra values with the time- and space-averaging of instantaneous fields. Note that the space-averaging was carried out only over an internal block of the grid that occupies a quarter of the cell diameter. Thus effects of the lateral wall were excluded. It is clearly seen formation of thin temperature boundary layers near the isothermal walls. Away from the walls a week inverse temperature gradient is registered. The thermal boundary layer thickness, δ_T, and the viscous boundary layer thickness, δ_V, were estimated taking the position at which the extrapolation of the linear part of the temperature (horizontal velocity) profile achieves the mean temperature at the mid-plane (the maximum horizontal velocity). Data on δ_T and δ_V obtained from the profiles taken at the central axis of the cell are listed in Table 1. The Prandtl number effect appears in the δ_T to δ_V ratio. For the mercury case, the viscous layer is nested within the thermal boundary layer. Results for water point to a reverse relation between δ_T and δ_V, i.e., the thermal boundary layer is considerably thinner than the viscous one. As shown in Figure 3 for mercury, the computed values of δ_T agree well with the power law fits, which are extrapolations of the experimental [15] and DNS [12] data.

Computed and measured [16] temperature fluctuations spectra in mercury for a point located away from the walls (z = 0.25) at the cell axis look similar (see Fig. 4). In particular one can observe a decay range with nearly the same power, $f^{-1.55}$, that is close to the Kolmogorov law. This result indicates that in low-Pr convection temperature behaves as a passive scalar in the flow core. The spectrum computed for water has an extended range of decreasing with the "7/5" law corresponding to buoyancy controlled turbulence in the regions away from the walls.

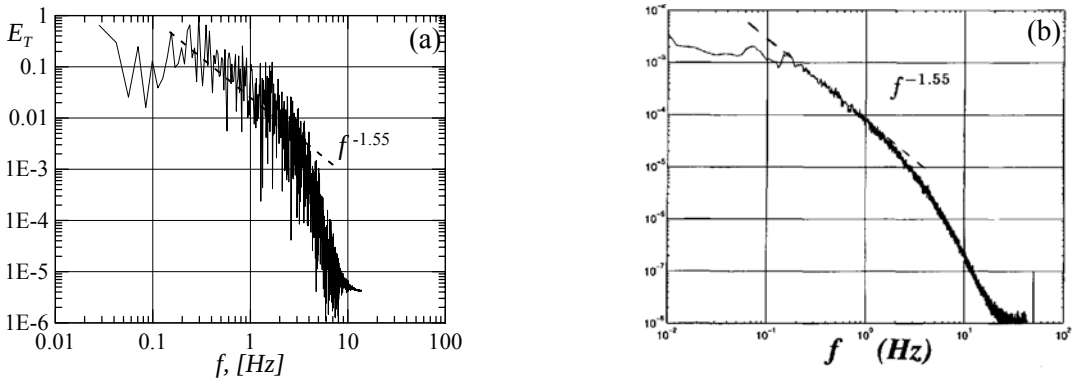

Fig. 4. Power spectral density of temperature fluctuations in mercury (z = 0.25). Comparison of (a) present RANS/LES results with (b) experiment [16]: Ra = 5×10^8

The above discussed features of the turbulent RB convection determine the heat transport across the cell. It should be emphasized also that contributions of the global circulation and thermal plumes to heat transfer change with varying the Prandtl number. For mercury, at moderate Ra the heat is mostly transported by the global circulation along the cell boundaries [12]. However, in strong turbulent regimes, $Ra \geq 10^8$, an increase in the Rayleigh number is accompanied by a decrease in the global circulation intensity. Consequently, the thermal plumes start to be formed in the convective flow and to take the role of an additional heat carrier. In the water convection, the heat is mainly transported by the thermal plumes, and the role of the global circulation is less significant [11].

Intensive 3D fluctuations exert influence on time evolution of integral heat flux through the horizontal walls of the cell (see Fig. 5). Against a background of predominant high frequencies one can see a presence of a low-frequency component of heat rate fluctuations that can be bound with the time scale of the global circulation.

Figure 6 shows that for both the fluids the Nusselt numbers computed are in a quantitative agreement with known experimental laws [16-18]. The present RANS/LES results obtained for mercury are very close to a fit from [18] that gives $Nu \propto Ra^{0.285}$ over a wide range of Ra, up to 8×10^{10}.

It is of interest to compare the RANS/LES results with computational data obtained on the base of other approaches to turbulence modeling. Considering the case of mercury convection at

$\mathrm{Ra} = 5\times10^8$, we performed also computations with the pure RANS approach using the well-known low-Re $k-\varepsilon$ model of Launder & Sharma (LS), and without any turbulence model (under-resolved DNS). One more run was carried out with artificial limitation of the turbulent viscosity, produced by the LS model, taking $\nu_t^{\mathrm{lim}} = \min\{\nu_t, 25\,\nu\}$.

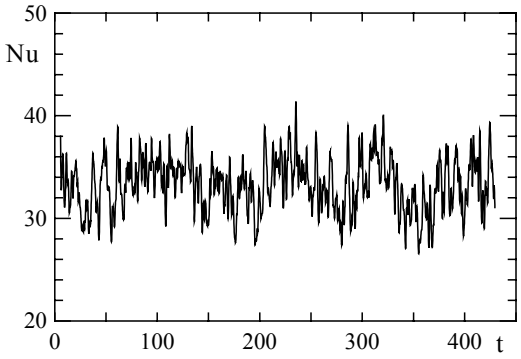

Fig. 5. Time evolution of heat rate through the horizontal walls. Mercury, $\mathrm{Ra} = 5\times10^8$

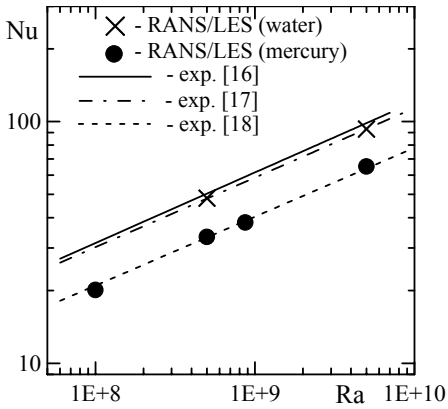

Fig. 6. Nusselt versus Rayleigh number in comparison with experimental data

Effect of turbulence modeling on the Nusselt number is illustrated by Table 2. The RANS/LES approach shows the best quantitative agreement with experiment [18]. Under-resolved DNS gives a value Nu that is about 15 percents smaller. A steady-state solution given by the pure RANS model predicts too high Nusselt numbers. The RANS with the limited turbulent viscosity allows a development of large-scale eddies, and leads to some improvement, as compared with the pure RANS model. Accounting for this fact, one could expect that RANS computations with various limit values of ν_t/ν are able to get Nu values that are close to experimental data. Obviously, that such an empiric method can not be considered as universal and reliable.

Table 2

Turbulence modelling effect on predicted Nusselt number in mercury convection, $\mathrm{Ra} = 5\times10^8$

Approach	Turbulence model	Nu
Experiment [18]	-	33.2
Under-resolved DNS	no	27.8
RANS/LES	one equation *k*-model	33.3
RANS	k-ε (without limitation of ν_t)	44.2
RANS	k-ε (with limitation of ν_t)	36.6

Conclusions

A numerical analysis of turbulent Rayleigh-Bénard convection in cells of aspect ratio 1 filled with mercury (cylindrical cell) or water (cubic cell) on the base of a hybrid RANS/LES technique was performed. The Rayleigh number was ranged from 10^8 to 5×10^9.

The development of a large-scale circulation and thermal plumes was observed in numerical solutions, in accordance with experimental findings. In mercury the global circulation is considerably more intensive than in water. On the contrary thermal plumes activity in mercury is noticeably weaker. The viscous and temperature boundary layer thicknesses estimated from time-averaged profiles of velocity and temperature agree well with experimental data.

A comparison of computed Nusselt numbers with measured data showed a good agreement with experimental laws for both the fluids.

The study has been supported by the Russian Foundation of Basic Research, grant 01-02-16697.

References

1. Smirnov E.M. Recent advances in numerical simulation of 3D unsteady convection controlled by buoyancy and rotation, CD-ROM Proc. of the 12th International Heat Transfer Conference, Grenoble, France, 2002, 12p.

2. Julien K., Legg S., McWilliams J., Werne J. Rapidly rotating turbulent Rayleigh-Bénard convection, J. Fluid Mech., 1996, 322, 243.

3. Kerr M.R., Herring J.R. Prandtl number dependence of Nusselt number in DNS, J. Fluid Mech., 2000, 419, 325.

4. Cabot W., Moin P. Approximate wall boundary conditions in the large-eddy simulation of high Reynolds number flow, Flow, Turbulence and Combustion, 1999, 63, 269.

5. Spalart P.R. Strategies for turbulence modelling and simulations, Int. J. Heat Fluid Flow, 2000, 21, 252.

6. Abramov A.G., Ivanov N.G., Smirnov E.M. Numerical study of high-Ra Rayleigh-Bénard mercury and water convection in confined enclosures using a hybrid RANS/LES technique, Proc. of the Eurotherm Seminar 74, Eindhoven, the Netherlands, ed. by H.C. de Lange and A.A. van Steenhoven, TUE, 2003, 33.

7. Piomelli U., Balaras E., Squires K.D., Spalart P.R. Interaction of the inner and outer layers in large-eddy simulations with wall-layer models, Proc. of the 5th Int. Symp. On Engineering Turbulence Modelling and Measurements, Mallorca, Spain, Elsevier, 2002, 307.

8. Abramov A.G. Large eddy simulation of turbulent convection in enclosures heated from below: variants and capabilities, Ph.D. thesis, St.-Petersburg State Polytechnic University, Saint-Petersburg, Russia, 2003 (in Russian).

9. Smirnov E.M. Solving the full Navier-Stokes equations for very-long-duct flows using the artificial compressibility method, CD-ROM Proc. of the ECCOMAS 2000 Conf., Barcelona, Spain, 2000, 17p.

10. Zocchi G., Moses E., Libchaber A. Coherent structures in turbulent convection, an experimental study, Physica A, 1990, 166, 387.

11. Belmonte A., Tilgner A., Libchaber A. Temperature and velocity boundary layers in turbulent convection, Phys. Rev. E, 1994, 50, 269.

12. Verzicco R., Camussi R. Prandtl number effects in convective turbulence, J. Fluid. Mech., 1999, 383, 55.

13. Abramov A.G., Korsakov A.B. Direct numerical simulation of turbulent mercury convection in axysimmetric enclosures including MHD effects, Proc. 3th Russian National Conference on Heat Exchange, MEI, Moscow, 2002, 3, 33 (in Russian).

14. Shang Z.-D., Xia K.-Q. Scaling of the velocity power spectra in turbulent thermal convection, Phys. Rev. E, 2001, 64, 065301(R).

15. Takeshita T., Segawa T., Glazier J.A., Sano M. Thermal turbulence in mercury, Phys. Rev. Lett., 1996, 76, 1465.

16. Cioni S., Ciliberto S., Sommeria J. Experimental study of high-Rayleigh-number convection in mercury and water, Dynamics of Atmospheres and Oceans, 1996, 24, 117.

17. Xin Y.-B., Xia K.-Q. Boundary layer length scales in convective turbulence, Phys. Rev. E, 1997, 56 (3), 3010.

18. Glazier J.A., Segawa T., Naert A., Sano M. Evidence against ‘ultrahard’ thermal turbulence at very high Rayleigh numbers, Nature, 1999, 398, 307.